

Moments of the Electron Energy Spectrum in Semileptonic B Decays at Belle

K. Abe,¹⁰ K. Abe,⁴⁶ N. Abe,⁴⁹ I. Adachi,¹⁰ H. Aihara,⁴⁸ M. Akatsu,²⁴ Y. Asano,⁵³
T. Aso,⁵² V. Aulchenko,² T. Aushev,¹⁴ T. Aziz,⁴⁴ S. Bahinipati,⁶ A. M. Bakich,⁴³
Y. Ban,³⁶ E. Barberio,²³ M. Barbero,⁹ A. Bay,²⁰ I. Bedny,² U. Bitenc,¹⁵ I. Bizjak,¹⁵
S. Blyth,²⁹ A. Bondar,² A. Bozek,³⁰ M. Bračko,^{22,15} J. Brodzicka,³⁰ T. E. Browder,⁹
M.-C. Chang,²⁹ P. Chang,²⁹ Y. Chao,²⁹ A. Chen,²⁶ K.-F. Chen,²⁹ W. T. Chen,²⁶
B. G. Cheon,⁴ R. Chistov,¹⁴ S.-K. Choi,⁸ Y. Choi,⁴² Y. K. Choi,⁴² A. Chuvikov,³⁷
S. Cole,⁴³ M. Danilov,¹⁴ M. Dash,⁵⁵ L. Y. Dong,¹² R. Dowd,²³ J. Dragic,²³ A. Drutskoy,⁶
S. Eidelman,² Y. Enari,²⁴ D. Epifanov,² C. W. Everton,²³ F. Fang,⁹ S. Fratina,¹⁵
H. Fujii,¹⁰ N. Gabyshev,² A. Garmash,³⁷ T. Gershon,¹⁰ A. Go,²⁶ G. Gokhroo,⁴⁴
B. Golob,^{21,15} M. Grosse Perdekamp,³⁸ H. Guler,⁹ J. Haba,¹⁰ F. Handa,⁴⁷ K. Hara,¹⁰
T. Hara,³⁴ N. C. Hastings,¹⁰ K. Hasuko,³⁸ K. Hayasaka,²⁴ H. Hayashii,²⁵ M. Hazumi,¹⁰
E. M. Heenan,²³ I. Higuchi,⁴⁷ T. Higuchi,¹⁰ L. Hinz,²⁰ T. Hojo,³⁴ T. Hokuue,²⁴
Y. Hoshi,⁴⁶ K. Hoshina,⁵¹ S. Hou,²⁶ W.-S. Hou,²⁹ Y. B. Hsiung,²⁹ H.-C. Huang,²⁹
T. Igaki,²⁴ Y. Igarashi,¹⁰ T. Iijima,²⁴ A. Imoto,²⁵ K. Inami,²⁴ A. Ishikawa,¹⁰ H. Ishino,⁴⁹
K. Itoh,⁴⁸ R. Itoh,¹⁰ M. Iwamoto,³ M. Iwasaki,⁴⁸ Y. Iwasaki,¹⁰ R. Kagan,¹⁴ H. Kakuno,⁴⁸
J. H. Kang,⁵⁶ J. S. Kang,¹⁷ P. Kapusta,³⁰ S. U. Kataoka,²⁵ N. Katayama,¹⁰ H. Kawai,³
H. Kawai,⁴⁸ Y. Kawakami,²⁴ N. Kawamura,¹ T. Kawasaki,³² N. Kent,⁹ H. R. Khan,⁴⁹
A. Kibayashi,⁴⁹ H. Kichimi,¹⁰ H. J. Kim,¹⁹ H. O. Kim,⁴² Hyunwoo Kim,¹⁷ J. H. Kim,⁴²
S. K. Kim,⁴¹ T. H. Kim,⁵⁶ K. Kinoshita,⁶ P. Koppenburg,¹⁰ S. Korpar,^{22,15} P. Krizan,^{21,15}
P. Krokovny,² R. Kulasiri,⁶ C. C. Kuo,²⁶ H. Kurashiro,⁴⁹ E. Kurihara,³ A. Kusaka,⁴⁸
A. Kuzmin,² Y.-J. Kwon,⁵⁶ J. S. Lange,⁷ G. Leder,¹³ S. E. Lee,⁴¹ S. H. Lee,⁴¹
Y.-J. Lee,²⁹ T. Lesiak,³⁰ J. Li,⁴⁰ A. Limosani,²³ S.-W. Lin,²⁹ D. Liventsev,¹⁴
J. MacNaughton,¹³ G. Majumder,⁴⁴ F. Mandl,¹³ D. Marlow,³⁷ T. Matsuishi,²⁴
H. Matsumoto,³² S. Matsumoto,⁵ T. Matsumoto,⁵⁰ A. Matyja,³⁰ Y. Mikami,⁴⁷
W. Mitaroff,¹³ K. Miyabayashi,²⁵ Y. Miyabayashi,²⁴ H. Miyake,³⁴ H. Miyata,³² R. Mizuk,¹⁴
D. Mohapatra,⁵⁵ G. R. Moloney,²³ G. F. Moorhead,²³ T. Mori,⁴⁹ A. Murakami,³⁹
T. Nagamine,⁴⁷ Y. Nagasaka,¹¹ T. Nakadaira,⁴⁸ I. Nakamura,¹⁰ E. Nakano,³³ M. Nakao,¹⁰
H. Nakazawa,¹⁰ Z. Natkaniec,³⁰ K. Neichi,⁴⁶ S. Nishida,¹⁰ O. Nitoh,⁵¹ S. Noguchi,²⁵
T. Nozaki,¹⁰ A. Ogawa,³⁸ S. Ogawa,⁴⁵ T. Ohshima,²⁴ T. Okabe,²⁴ S. Okuno,¹⁶ S. L. Olsen,⁹
Y. Onuki,³² W. Ostrowicz,³⁰ H. Ozaki,¹⁰ P. Pakhlov,¹⁴ H. Palka,³⁰ C. W. Park,⁴² H. Park,¹⁹
K. S. Park,⁴² N. Parslow,⁴³ L. S. Peak,⁴³ M. Pernicka,¹³ J.-P. Perroud,²⁰ M. Peters,⁹
L. E. Piilonen,⁵⁵ A. Poluektov,² F. J. Ronga,¹⁰ N. Root,² M. Rozanska,³⁰ H. Sagawa,¹⁰
M. Saigo,⁴⁷ S. Saitoh,¹⁰ Y. Sakai,¹⁰ H. Sakamoto,¹⁸ T. R. Sarangi,¹⁰ M. Satapathy,⁵⁴
N. Sato,²⁴ O. Schneider,²⁰ J. Schümann,²⁹ C. Schwanda,¹³ A. J. Schwartz,⁶ T. Seki,⁵⁰
S. Semenov,¹⁴ K. Senyo,²⁴ Y. Settai,⁵ R. Seuster,⁹ M. E. Sevier,²³ T. Shibata,³²
H. Shibuya,⁴⁵ B. Shwartz,² V. Sidorov,² V. Siegle,³⁸ J. B. Singh,³⁵ A. Somov,⁶ N. Soni,³⁵
R. Stamen,¹⁰ S. Stanič,^{53,*} M. Starič,¹⁵ A. Sugi,²⁴ A. Sugiyama,³⁹ K. Sumisawa,³⁴
T. Sumiyoshi,⁵⁰ S. Suzuki,³⁹ S. Y. Suzuki,¹⁰ O. Tajima,¹⁰ F. Takasaki,¹⁰ K. Tamai,¹⁰
N. Tamura,³² K. Tanabe,⁴⁸ M. Tanaka,¹⁰ G. N. Taylor,²³ Y. Teramoto,³³ X. C. Tian,³⁶

S. Tokuda,²⁴ S. N. Tovey,²³ K. Trabelsi,⁹ T. Tsuboyama,¹⁰ T. Tsukamoto,¹⁰
 K. Uchida,⁹ S. Uehara,¹⁰ T. Uglov,¹⁴ K. Ueno,²⁹ Y. Unno,³ S. Uno,¹⁰ P. Urquijo,²³
 Y. Ushiroda,¹⁰ G. Varner,⁹ K. E. Varvell,⁴³ S. Villa,²⁰ C. C. Wang,²⁹ C. H. Wang,²⁸
 J. G. Wang,⁵⁵ M.-Z. Wang,²⁹ M. Watanabe,³² Y. Watanabe,⁴⁹ L. Widhalm,¹³
 Q. L. Xie,¹² B. D. Yabsley,⁵⁵ A. Yamaguchi,⁴⁷ H. Yamamoto,⁴⁷ S. Yamamoto,⁵⁰
 T. Yamanaka,³⁴ Y. Yamashita,³¹ M. Yamauchi,¹⁰ Heyoung Yang,⁴¹ P. Yeh,²⁹ J. Ying,³⁶
 K. Yoshida,²⁴ Y. Yuan,¹² Y. Yusa,⁴⁷ H. Yuta,¹ S. L. Zang,¹² C. C. Zhang,¹² J. Zhang,¹⁰
 L. M. Zhang,⁴⁰ Z. P. Zhang,⁴⁰ V. Zhilich,² T. Ziegler,³⁷ D. Žontar,^{21,15} and D. Zürcher²⁰

(The Belle Collaboration)

¹*Aomori University, Aomori*

²*Budker Institute of Nuclear Physics, Novosibirsk*

³*Chiba University, Chiba*

⁴*Chonnam National University, Kwangju*

⁵*Chuo University, Tokyo*

⁶*University of Cincinnati, Cincinnati, Ohio 45221*

⁷*University of Frankfurt, Frankfurt*

⁸*Gyeongsang National University, Chinju*

⁹*University of Hawaii, Honolulu, Hawaii 96822*

¹⁰*High Energy Accelerator Research Organization (KEK), Tsukuba*

¹¹*Hiroshima Institute of Technology, Hiroshima*

¹²*Institute of High Energy Physics,*

Chinese Academy of Sciences, Beijing

¹³*Institute of High Energy Physics, Vienna*

¹⁴*Institute for Theoretical and Experimental Physics, Moscow*

¹⁵*J. Stefan Institute, Ljubljana*

¹⁶*Kanagawa University, Yokohama*

¹⁷*Korea University, Seoul*

¹⁸*Kyoto University, Kyoto*

¹⁹*Kyungpook National University, Taegu*

²⁰*Swiss Federal Institute of Technology of Lausanne, EPFL, Lausanne*

²¹*University of Ljubljana, Ljubljana*

²²*University of Maribor, Maribor*

²³*University of Melbourne, Victoria*

²⁴*Nagoya University, Nagoya*

²⁵*Nara Women's University, Nara*

²⁶*National Central University, Chung-li*

²⁷*National Kaohsiung Normal University, Kaohsiung*

²⁸*National United University, Miao Li*

²⁹*Department of Physics, National Taiwan University, Taipei*

³⁰*H. Niewodniczanski Institute of Nuclear Physics, Krakow*

³¹*Nihon Dental College, Niigata*

³²*Niigata University, Niigata*

³³*Osaka City University, Osaka*

³⁴*Osaka University, Osaka*

³⁵*Panjab University, Chandigarh*

³⁶*Peking University, Beijing*

- ³⁷*Princeton University, Princeton, New Jersey 08545*
³⁸*RIKEN BNL Research Center, Upton, New York 11973*
³⁹*Saga University, Saga*
⁴⁰*University of Science and Technology of China, Hefei*
⁴¹*Seoul National University, Seoul*
⁴²*Sungkyunkwan University, Suwon*
⁴³*University of Sydney, Sydney NSW*
⁴⁴*Tata Institute of Fundamental Research, Bombay*
⁴⁵*Toho University, Funabashi*
⁴⁶*Tohoku Gakuin University, Tagajo*
⁴⁷*Tohoku University, Sendai*
⁴⁸*Department of Physics, University of Tokyo, Tokyo*
⁴⁹*Tokyo Institute of Technology, Tokyo*
⁵⁰*Tokyo Metropolitan University, Tokyo*
⁵¹*Tokyo University of Agriculture and Technology, Tokyo*
⁵²*Toyama National College of Maritime Technology, Toyama*
⁵³*University of Tsukuba, Tsukuba*
⁵⁴*Utkal University, Bhubaneswer*
⁵⁵*Virginia Polytechnic Institute and State University, Blacksburg, Virginia 24061*
⁵⁶*Yonsei University, Seoul*

Abstract

We report a measurement of the inclusive electron energy spectrum for semileptonic decays of B mesons in a 140 fb^{-1} data sample collected near the $\Upsilon(4S)$ resonance, with the Belle detector at the KEKB asymmetric energy e^+e^- collider. We determine the first and second moments of the spectrum for threshold values of the electron energy between 0.6 and 1.5 GeV.

PACS numbers: 12.15.Hh, 11.30.Er, 13.25.Hw

INTRODUCTION

The Cabibbo-Kobayashi-Maskawa matrix element $|V_{cb}|$ can be extracted from the inclusive branching fraction for semileptonic b hadron decays $B(B \rightarrow X_c \ell \nu)$ [1, 2]. Several studies have shown that the spectator model decay rate is the leading term in a well-defined expansion controlled by the parameter Λ_{QCD}/m_b . Non-perturbative corrections to this leading approximation arise only at order $1/m_b^2$ and above. The key issue in this approach is the ability to separate non-perturbative corrections, which can be expressed as a series in powers of $1/m_b$, and perturbative corrections, expressed in powers of α_s .

The coefficients of the $1/m_b$ power terms are expectation values of operators that include non-perturbative physics. Two different expansions exist, reflecting a difference in the approach used to handle the energy scale μ that separates long-distance from short-distance physics. In this note, we use the short distant mass expansion that defines the non-perturbative operators using a mass scale $\mu \approx 1 \text{ GeV}$ [3].

The shape of the lepton spectrum provides constraints on the heavy quark expansion based on local Operator Product Expansion (OPE), which calculates properties of the $B \rightarrow X_c \ell \nu$ transitions. So far, measurements of the electron energy distribution have been made by the DELPHI, CLEO, and BABAR collaborations [4, 5, 6]. In this note we report a measurement of the first and second moment of the electron energy spectrum with a minimum electron momentum cut ranging between 0.6 and 1.5 GeV in the B meson rest frame. We measure, independently, the electron energy moments for the semileptonic decays of the B^+ and the B^0 mesons [7]. If quark hadron duality applies in $B \rightarrow X_c \ell \nu$ decays then the moments from the B^+ and B^0 should agree. Up to now such a measurement has been impossible to perform. However, in this measurement we find good agreement between the moments.

The data used in this analysis was collected with the Belle detector at the KEKB [8] asymmetric energy e^+e^- collider. The Belle [9] detector is a large-solid-angle magnetic spectrometer that consists of a three-layer silicon vertex detector (SVD), a 50-layer central drift chamber (CDC), an array of aerogel threshold Čerenkov counters (ACC), a barrel-like arrangement of time-of-flight scintillation counters (TOF), and an electromagnetic calorimeter comprised of CsI(Tl) crystals (ECL) located inside a super-conducting solenoid coil that provides a 1.5 T magnetic field. An iron flux-return located outside of the coil is instrumented to detect K_L^0 mesons and to identify muons (KLM).

Events are selected by fully reconstructing one of the B mesons, produced in pairs from $\Upsilon(4S)$, in several hadronic decay modes. Prompt semileptonic decays ($b \rightarrow x \ell \nu$) of the non-tag side B mesons are separated from cascade charm decays ($b \rightarrow c \rightarrow y \ell \nu$), based on the correlation between the flavour of the tagged B and the lepton charge.

The present results are based on a 140 fb^{-1} data sample collected at the $\Upsilon(4S)$ resonance, which contains 1.5×10^8 $B\bar{B}$ pairs. An additional 15 fb^{-1} data sample taken at 60 MeV below the $\Upsilon(4S)$ resonance (off-resonance) is used to perform background subtraction from the $e^+e^- \rightarrow q\bar{q}$ process.

We use a fully simulated generic Monte Carlo sample generated with the qq98 event generator [10]. This sample is equivalent to about three times the beam luminosity of the real data. Simulated events are required to satisfy tight hadron selection criteria.

FULL RECONSTRUCTION SAMPLE

The hadronic decay of the tag-side B meson is fully reconstructed in the decay modes $B \rightarrow D^{(*)}\pi^+, D^{(*)}\rho^+, D^{(*)}a_1^+$, yielding a high purity B meson sample. The following sub-decay modes are implemented:

- $D^{*0} \rightarrow D^0\pi^0, D^0\gamma,$
- $D^{*+} \rightarrow D^0\pi^+, D^+\pi^0,$
- $D^0 \rightarrow K\pi, K\pi\pi^0, K\pi\pi\pi, K_S\pi\pi, K_S\pi^0$ and
- $D^+ \rightarrow K\pi\pi, K_S\pi.$

If multiple candidates are found in one event, we select the best candidate based on ΔE and other variables. There are two conditions that affect the best candidate selection. The candidate may be reconstructed from at least one particle from the other side B , or the final state particles may be incorrectly reconstructed.

ELECTRON SELECTION

We identify electrons produced in semileptonic B decays on the “non-tag” side. Low-momentum particles spiral in the CDC detector. If the particles pass close to the interaction point more than once, they can lead to multiple reconstructed tracks. Those tracks are removed. The remaining tracks are required to satisfy tight restrictions on the impact parameters. In addition, we require the tracks to be in the barrel region of the detector, corresponding to an angular acceptance of $35^\circ \leq \theta_{\text{lab}} \leq 125^\circ$, where θ_{lab} is the polar angle of the track relative to the z axis (opposite the positron beam line).

Tracks that pass the above selection criteria and are not used in the reconstruction of the tag-side B meson are considered as electron candidates. Electron identification is based on a combination of specific ionisation dE/dx measurements in the CDC, the response of the ACC, the shower shape in the ECL, and the ratio of energy deposit in the ECL to the momentum measured by the tracking system (E/p) [9]. The electron identification efficiencies include the detector acceptance as well as the selection efficiency. The errors for the tracking and electron detection efficiencies are $\pm 1\%$ and $\pm 2\%$, respectively. Electron identification efficiency is determined by analysing a data sample where simulated single electron tracks are overlaid on hadronic events taken from real experimental data. The electron momentum spectrum is corrected by using this momentum dependent electron detection efficiency.

The momentum of electron candidates is measured in the B meson rest frame ($p^{*(B)}$), exploiting the knowledge on the momentum of the fully reconstructed B . To ensure a good electron identification performance we require $p_e^{*(B)} \geq 0.6 \text{ GeV}/c$.

Backgrounds from J/ψ , $\psi(2S)$, photon conversions in the material of the detector, and Dalitz decays from π^0 and η mesons are reduced by imposing veto cuts. We look for additional electrons in the event, which satisfy looser identification criteria and $p_e \geq 0.3 \text{ GeV}/c$. We then calculate invariant masses (m_{ee}) for each electron candidate when combined with an opposite-charge electron that passes the loose selection. In the Dalitz case we require an additional photon ($m_{ee\gamma}$). We reject the electron if m_{ee} lies within the nominal J/ψ and

$\psi(2S)$ mass regions, or $m_{ee\gamma}$ lies within the nominal π^0 and η mass regions. To remove photon conversions we reject candidates by placing cuts on the vertex of the decay and m_{ee} less than $100 \text{ MeV}/c^2$.

NUMBER OF TAGGED EVENTS

We select events containing a fully reconstructed B candidate on one side and an electron candidate on the other side.

For each selected event, we calculate the beam-constrained mass M_{bc} and ΔE :

$$M_{bc} = \sqrt{(E_{\text{beam}}^*)^2 - (\vec{p}_B^*)^2}, \quad \Delta E = E_B^* - E_{\text{beam}}^*, \quad (1)$$

where E_{beam}^* , \vec{p}_B^* and E_B^* are the beam energy, the B 3-momentum and the B energy in the centre of mass frame, respectively. Events with $M_{bc} > 5.27 \text{ GeV}/c^2$ and $-0.06 \text{ GeV} < \Delta E < 0.08 \text{ GeV}$ are considered to be signal candidates.

Each electron is assigned to the “right sign” sample if the electron has the opposite flavour to the fully reconstructed B , and to the “wrong sign” sample if the electron has the same flavour as the fully reconstructed B . In events without $B^0\bar{B}^0$ mixing, the primary electrons belong to the “right sign” sample while the secondary electrons contribute to the “wrong sign” sample. Figure 1 shows the beam constrained mass distribution for B^0 and B^+ right sign and B^0 wrong sign electrons, with scaled off resonance background overlaid. The number of events in the signal region, is 3367 ± 58 (1659 ± 40) and 6831 ± 83 for the B^0 right sign (wrong sign) and B^+ right sign candidates, respectively.

BACKGROUND SUBTRACTION

The selected electron energy spectrum is contaminated by background processes, which should be evaluated and subtracted from the distribution before the extraction of the moments. The residual background is from:

- continuum background,
- full-reconstruction background,
- background from secondary decays,
- $J/\psi, \psi(2S)$, Dalitz decays and photon conversions where one electron of the pair has escaped detection and
- fake electrons.

The electron momentum spectrum of the continuum background is derived from off-resonance data and is normalised using the off- to on-resonance luminosity ratio. To account for the low statistics in the off-resonance data we fit an exponential to the electron energy distribution. We fit only the B^+ candidates then apply the same continuum cut to the B^0 , scaled to the electron yield of the wrong sign and right sign B^0 samples. There are insufficient statistics to fit the off-resonance B^0 samples.

The electron momentum spectrum of the combinatorial background is derived from the generic $B\bar{B}$ Monte Carlo events where either reconstruction or flavour assignment of the

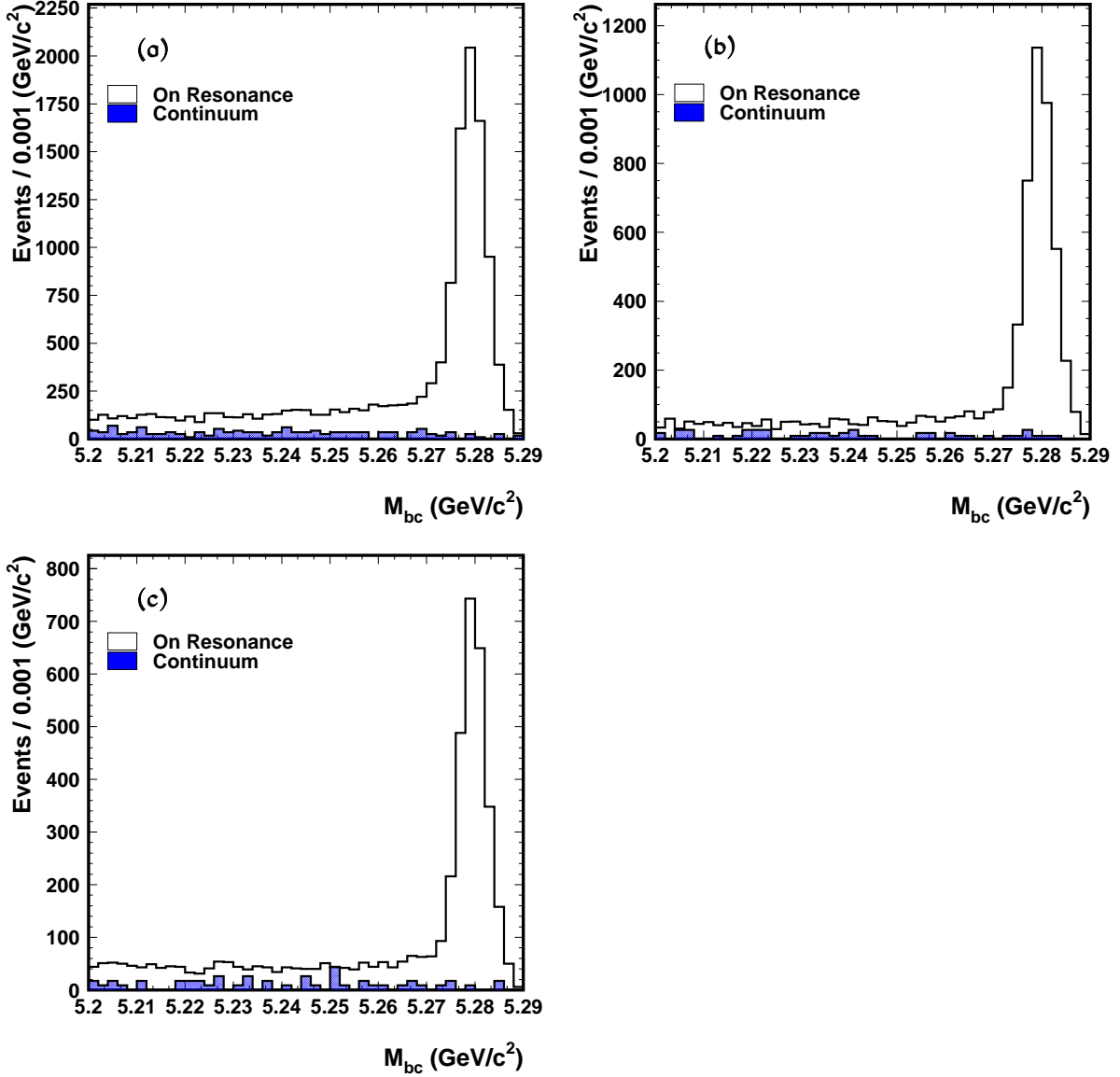


FIG. 1: The beam constrained mass after electron selection cuts and ΔE cuts for the B^+ right sign electron sample (a), B^0 right sign electron sample (b) and the B^0 wrong sign electron sample (c).

tagged B meson is not carried out correctly. The $B\bar{B}$ Monte Carlo events are normalised to the on resonance data M_{bc} side band ($M_{bc} < 5.25 \text{ GeV}/c^2$) after continuum background subtraction in this region.

We also correct for cases where the fully reconstructed B is correctly tagged, but the electron does not directly originate from a B decay or is a hadron misidentified as an electron. These backgrounds are irreducible; to estimate the magnitude of the contributions we normalise the $B\bar{B}$ Monte Carlo to the electron yield after continuum and combinatorial background subtraction.

Secondary electrons arising from $B \rightarrow D^{(*)} \rightarrow e$, $B \rightarrow \tau \rightarrow e$, and $B \rightarrow D^{(*)} \rightarrow \tau \rightarrow e$ decays are simulated using the latest published branching fractions [14].

Contributions from $J/\psi, \psi(2S)$ decays, photon conversions, and Dalitz decays are insignificant after the electron selection cuts. The surviving backgrounds, where one electron of the pair has escaped detection, are estimated by the Monte Carlo simulation and subtracted along with the major secondary backgrounds.

The Monte Carlo yield due to fakes is corrected for the difference in the fake rate for data and Monte Carlo measured with samples of $K_S^0 \rightarrow \pi^+\pi^-$ decays. The magnitude of the correction is assigned as the systematic uncertainty on the fake yield.

Figure 2 shows the raw electron momentum spectrum with all background contributions overlaid. Table I summarises the number of detected electrons and the contributions from these backgrounds.

MIXING CORRECTIONS

To reduce the contamination from cascade semileptonic charm decays, we determine whether the electron's parent and the fully reconstructed B have the same or opposite flavour. For events tagged as B^+ we require the right sign tag. For events tagged as B^0 , we introduce a dependence on $B^0\bar{B}^0$ mixing which is taken into account by solving the equations; $N_{\text{right}} = N_p(1 - \chi_d) + N_c\chi_d$, $N_{\text{wrong}} = N_p\chi_d + N_c(1 - \chi_d)$ where N_{right} and N_{wrong} are the number of electrons with the right and wrong signs, respectively. N_p and N_c are the number of electrons from the prompt and cascade semileptonic decays, respectively and $\chi_d = 0.186 \pm 0.004$ [14] is the mixing probability.

CORRECTIONS TO THE ELECTRON ENERGY SPECTRUM

The electron energy spectrum is generated via Monte Carlo simulation of $B \rightarrow X_c e \nu$ decays using the qq98 event generator [10]. The spectrum from $B \rightarrow X_c e \nu$ is modelled using four components: $X_c = D$ (ISGW2 [11]), D^* (HQET [12]), higher resonance charm meson states D^{**} (ISGW2) and non-resonant $D^{(*)}\pi$ (Goity and Roberts [13]). To account for the most recent theoretical and experimental results, we re-weight the D and D^* components in $p^{*(B)}$ to the spectra generated with current world average form factors [14].

The available Monte Carlo sample does not incorporate $\mathcal{O}(\alpha)$ QED corrections. We correct the background subtracted electron spectrum with energy-dependent weights using the PHOTOS [15] package.

Electrons that come from the $b \rightarrow u$ transition are subtracted from the unfolded electron energy spectrum, defined later. We model the electron energy spectrum from the $B \rightarrow X_u l \nu$ using the De Fazio and Neubert prescription [16]. The b -quark motion parameters are derived in Ref. [17]. We scale according to the $B \rightarrow X_u l \nu$ branching fraction in Ref. [14].

The electron momentum spectra, after all corrections have been applied, are shown in Figure 3.

UNFOLDING THE ELECTRON ENERGY SPECTRUM

To measure the first and second electron moments we need to determine the true electron energy spectrum. The background subtracted energy spectrum is distorted by various detector effects. The true electron energy spectrum is extracted by performing an unfolding

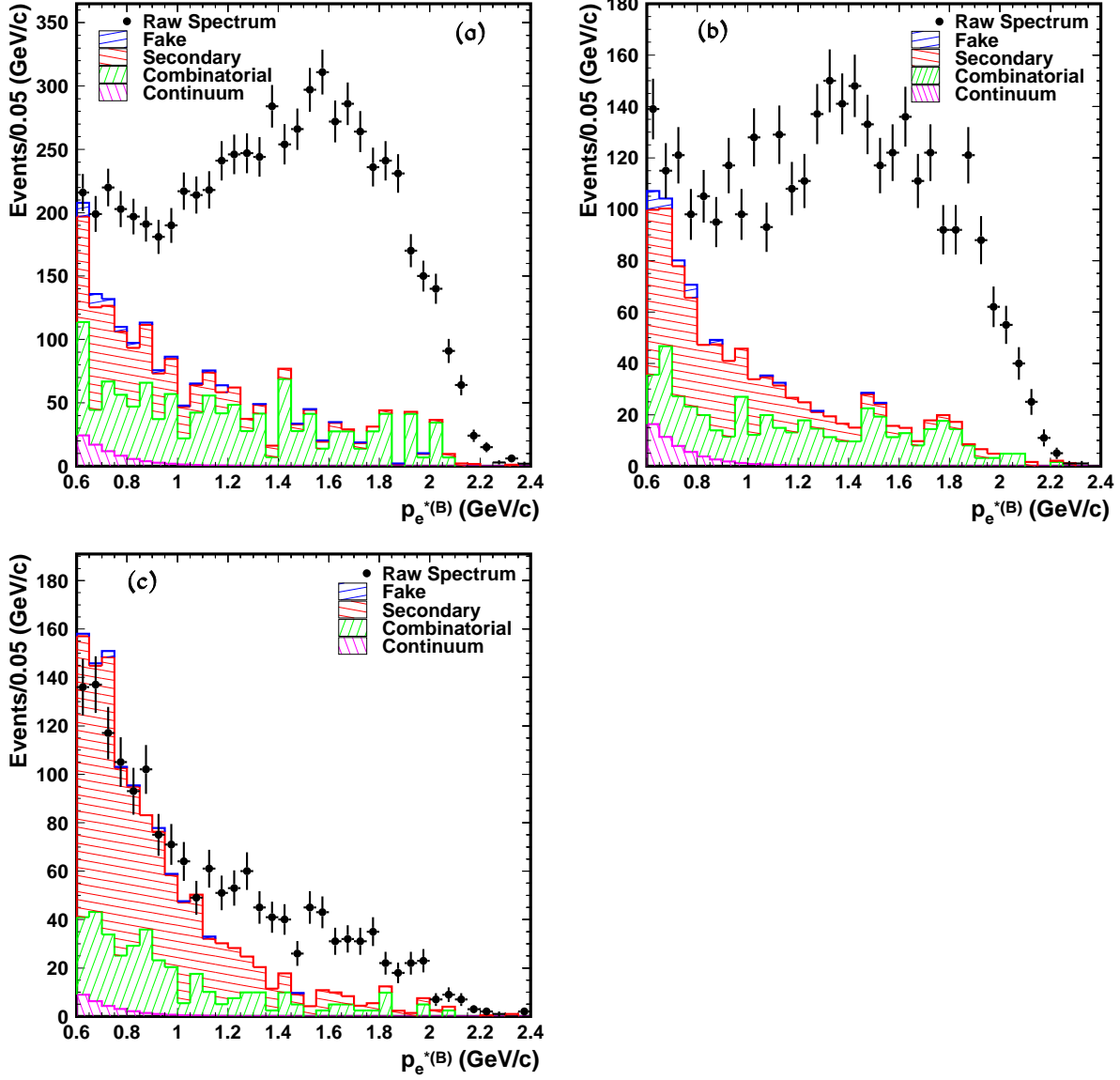


FIG. 2: Breakdown of the backgrounds in the electron momentum spectra for B^+ right sign (a), B^0 right sign (b) and B^0 wrong sign (c) electrons.

procedure based on the Singular Value Decomposition (SVD) algorithm of A.Höcker and V. Kartvelishvili [18].

Figure 4 shows the correlation between the reconstructed and generated electron energy. Due to the good resolution of the Belle detector, the reconstructed electron energy is highly correlated with the generated one. The off-diagonal bins are filled due to bremsstrahlung occurring in the material in front of the calorimeter. It is important to note, for the reliability of the unfolding, that the phase space covered by the generated energy spectrum is very similar to the reconstructed spectrum.

We divide the generated energy in slices of 0.025 GeV. For each slice we produce a histogram of the corresponding reconstructed energy spectrum, normalised to one. The histogram has a bin width of 0.025 GeV. Bin and slicing widths have been chosen to have less than 40% correlation (cross-talk) between bins and/or slices. These histograms are then

TABLE I: Number of Electrons

B candidate	B^0 right-sign	B^0 wrong-sign	B^+ right-sign
On Resonance Data	3367 ± 58	1659 ± 40	6831 ± 83
Scaled Off Resonance	54 ± 7	30 ± 6	106 ± 10
Combinatorial Background	420 ± 26	339 ± 29	1073 ± 86
$B\bar{B}$ Background	479 ± 21	856 ± 29	688 ± 23
Secondary	456 ± 20	847 ± 29	634 ± 23
Hadron Fakes	23 ± 4	9 ± 2	54 ± 5
Background Subtracted	2414 ± 67	434 ± 58	4964 ± 122
After Efficiency Correction	4066 ± 115	727 ± 100	8371 ± 209
After Mixing Correction	5054 ± 145	N/A	N/A

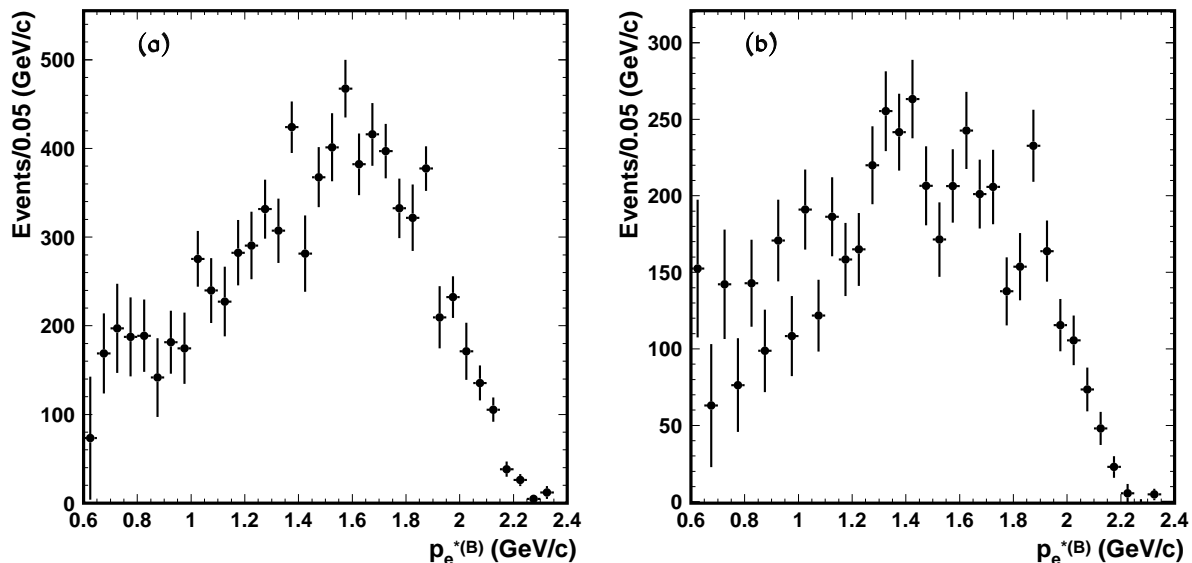


FIG. 3: The electron momentum spectrum in the B rest frame after background subtraction, mixing and efficiency correction for B^+ (a) and B^0 (b).

used to generate a response matrix. Next, we use the SVD algorithm to perform singular value (eigenvalue) analysis of the response matrix. Figure 5 compares the unfolded Monte Carlo electron energy spectrum compared to the true spectrum.

We weight the Monte Carlo spectra with the QED radiative effects in order to calculate the correct unfolding matrix. When we unfold the data we remove the QED radiative effects, as the OPE does not have an $\mathcal{O}(\alpha)$ QED correction. The unfolded electron energy spectrum for data is shown in Figure 6.

MOMENTS OF THE ELECTRON ENERGY SPECTRUM

The first moment of the electron energy spectrum is defined to be $M_1^e(E_{\text{cut}}) = \langle E_e \rangle_{E_e > E_{\text{cut}}}$ and the second $M_2^e(E_{\text{cut}}) = \langle (E_e - M_1^e(E_{\text{cut}}))^2 \rangle_{E_e > E_{\text{cut}}}$. We measure the first and second

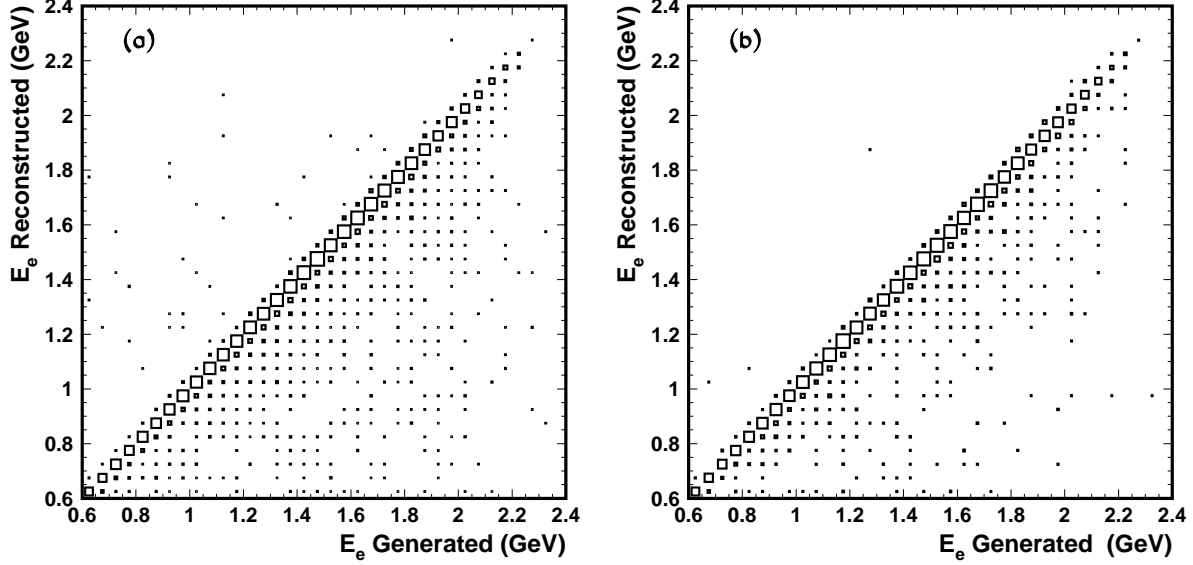


FIG. 4: Correlation between reconstructed and generated electron energy (i.e. reconstructed versus generated electron energy spectrum) for B^+ (a) and B^0 (b). The high population in the diagonal bins demonstrates the high resolution in the unfolding procedure.

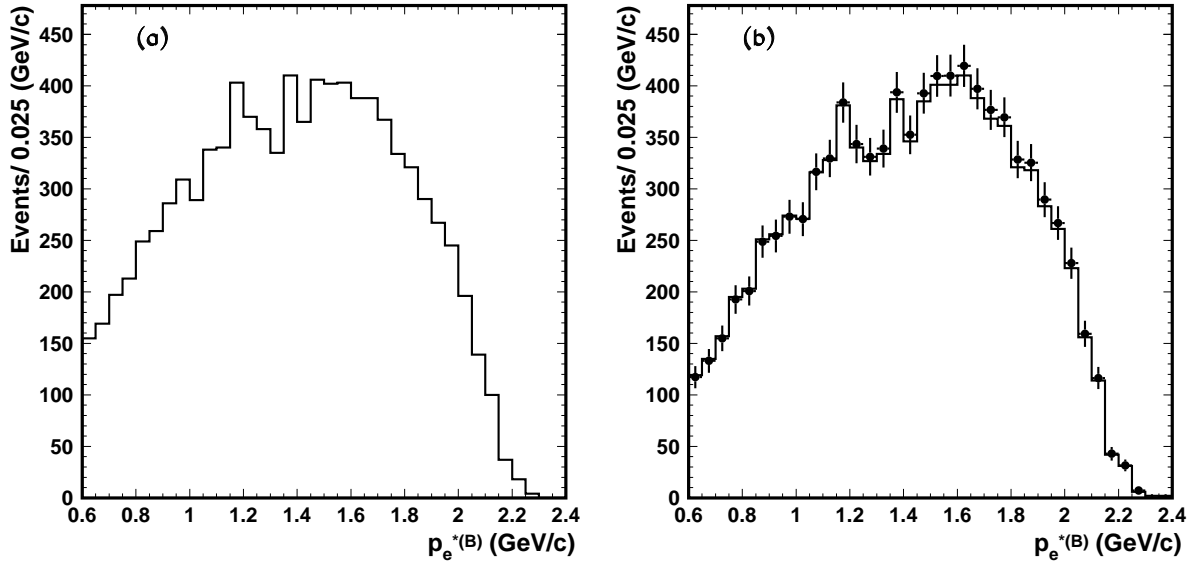


FIG. 5: Generated and unfolded E_e distributions for Monte Carlo simulated events (b). The reconstructed electron spectrum after the detector simulation is show in (a). The continuous line in (b) is the true (generator level) E_e distribution. The unfolded distribution is overlaid (data points).

moments with five electron energy threshold cuts ($E_{\text{cut}} = 0.6, 0.8, 1.0, 1.2$ and 1.5 GeV) for the B^+ and B^0 mesons. Table IV gives the final measurements of the moments, with radiative corrections applied.

Figure 7 shows the measured moments for the B^0 and B^+ data samples with the theoretical bounds as a function of the threshold electron energy. The theoretical bounds in

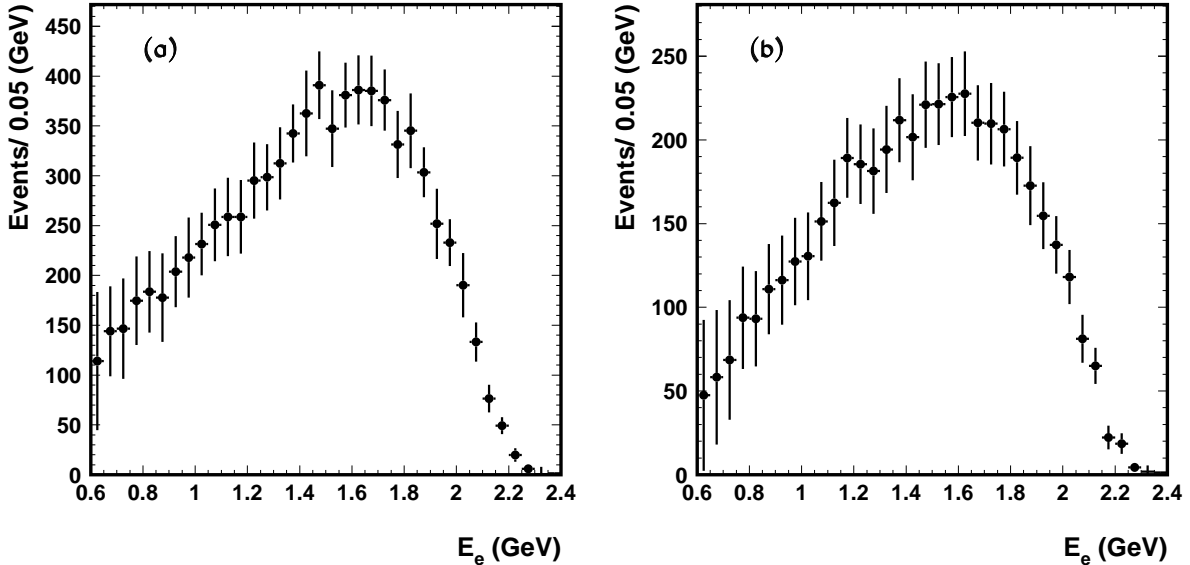


FIG. 6: Unfolded E_e distribution corrected for QED radiative effects for B^+ (a) and B^0 (b). The errors shown are statistical.

Figure 7 are taken from Ref. [3], in the kinetic mass scheme.

SYSTEMATIC UNCERTAINTIES

The systematic uncertainty in the moments stems from event selection, electron identification, background estimation, model dependence, and mixing.

The uncertainty due to mis-tagging in the B^0 and B^+ samples is derived from the magnitude of the combinatorial background and is estimated to be $\pm 2\%$. Uncertainty in the measured luminosity provides an uncertainty on the continuum electron yield of $\pm 1\%$.

The effect of veto cuts has been calculated as the quadratic sum of averaged variations in the moments when selection criteria are loosened and tightened about their chosen positions.

Subtraction of $b \rightarrow u$ decays acquires an uncertainty associated with the renormalisation to the full inclusive spectra. The renormalisation factor is varied by $\pm 50\%$.

The uncertainty in secondary ($B \rightarrow D \rightarrow e$) decays derives from uncertainty in the value of the branching fractions. Model dependence is estimated from the observed change in the moments when the $B \rightarrow De\nu$ and $B \rightarrow D^*e\nu$ decay shape parameters are varied.

The uncertainty in the mixing probability χ_d is based on the current quoted error in Ref. [14].

In addition, we calculate systematic uncertainty associated with the magnitude of the hadron fake contribution, electron tracking efficiency, and electron detection efficiency.

The total systematic error is obtained by adding each contribution in quadrature. It is important to note that the systematic errors are limited by Monte Carlo statistics, most significantly in the B^0 sample. The contributions to the systematic error are summarised in table II (B^+), and table III (B^0).

TABLE II: Breakdown of the systematic errors for the moments, M_1 , M_2 for $B^+ \rightarrow X_c e \nu$ in the B meson rest frame for 3 values of E_{cut}

$E_{\text{cut}}[\text{GeV}]$	M_1	M_1	M_1	M_2	M_2	M_2
	[MeV]	[MeV]	[MeV]	[10^3MeV^2]	[10^3MeV^2]	[10^3MeV^2]
	0.6	1.0	1.5	0.6	1.0	1.5
conversions and Dalitz decays	0.02	0.12	0.04	0.07	0.00	0.00
e from J/ψ or $\psi(2S)$	0.91	0.67	0.63	0.32	0.15	0.06
$B \rightarrow D_{(s)}^{(*)} \rightarrow e$	1.89	0.43	0.02	0.65	0.11	0.00
$D^{(*)}$	0.02	0.01	0.00	0.00	0.00	0.00
$b \rightarrow u$ subtraction	0.17	0.18	0.19	0.09	0.08	0.06
continuum background	0.00	0.00	0.00	0.00	0.00	0.00
combinatorial background	1.58	0.57	0.01	0.42	0.10	0.00
hadron fakes	1.24	0.20	0.01	0.47	0.06	0.00
electron detection	0.01	0.01	0.01	0.00	0.01	0.00
tracking efficiency	0.00	0.0	0.0	0.0	0.0	0.0
total systematics	3.59	1.13	0.67	1.21	0.27	0.09

TABLE III: Breakdown of the systematic errors for the moments, M_1 , M_2 for $B^0 \rightarrow X_c e \nu$ in the B meson rest frame for 3 values of E_{cut}

$E_{\text{cut}}[\text{GeV}]$	M_1	M_1	M_1	M_2	M_2	M_2
	[MeV]	[MeV]	[MeV]	[10^3MeV^2]	[10^3MeV^2]	[10^3MeV^2]
	0.6	1.0	1.5	0.6	1.0	1.5
conversions and Dalitz decays	0.02	0.26	0.17	0.21	0.06	0.01
e from J/ψ or $\psi(2S)$	0.40	0.25	0.51	0.45	0.20	0.01
$B \rightarrow D_{(s)}^{(*)} \rightarrow e$	2.38	0.77	0.05	0.71	0.13	0.00
χ	0.02	0.00	0.01	0.01	0.01	0.00
$D^{(*)}$	0.18	0.03	0.00	0.07	0.01	0.00
$b \rightarrow u$ subtraction	0.38	0.37	0.37	0.18	0.16	0.12
continuum background	0.00	0.00	0.00	0.00	0.00	0.00
combinatorial background	0.85	0.31	0.14	0.20	0.00	0.02
hadron fakes	0.93	0.17	0.01	0.34	0.03	0.00
electron detection	0.12	0.01	0.01	0.06	0.01	0.00
tracking efficiency	0.06	0.00	0.01	0.03	0.00	0.01
total systematics	2.76	0.99	0.67	0.97	0.30	0.12

SUMMARY

We report a measurement of the electron energy spectrum of the inclusive decay $B \rightarrow X_c e \nu$ and its first and second moments for threshold energies from 0.6 GeV to 1.5 GeV. This set of moments, combined with the measurements of the semileptonic branching fraction and

TABLE IV: Measured moments, M_1 , M_2 for $B \rightarrow X_c e \nu$ in the B meson rest frame for five cutoff energies E_{cut} . The first error is the statistical, and the second error is the systematic. The moments are corrected for QED radiative effects (using the PHOTOS package).

$E_{\text{cut}}[\text{GeV}]$	$M_1[\text{MeV}]$	$M_1[\text{MeV}]$	$M_2[10^3\text{MeV}^2]$	$M_2[10^3\text{MeV}^2]$
	B^+	B^0	B^+	B^0
0.6	$1432.1 \pm 4.3 \pm 3.6$	$1444.9 \pm 5.5 \pm 2.8$	$150.1 \pm 1.8 \pm 1.2$	$144.0 \pm 2.1 \pm 1.0$
0.8	$1487.2 \pm 3.9 \pm 2.2$	$1488.0 \pm 5.1 \pm 1.8$	$118.4 \pm 1.4 \pm 0.7$	$119.0 \pm 1.8 \pm 0.6$
1.0	$1554.1 \pm 3.6 \pm 1.1$	$1551.5 \pm 4.7 \pm 1.0$	$88.1 \pm 1.1 \pm 0.3$	$90.7 \pm 1.4 \pm 0.3$
1.2	$1631.7 \pm 3.3 \pm 0.7$	$1632.6 \pm 4.3 \pm 0.8$	$61.7 \pm 0.8 \pm 0.1$	$64.1 \pm 1.1 \pm 0.2$
1.5	$1774.8 \pm 2.8 \pm 0.7$	$1778.2 \pm 3.8 \pm 0.7$	$30.6 \pm 0.5 \pm 0.1$	$32.3 \pm 0.7 \pm 0.1$

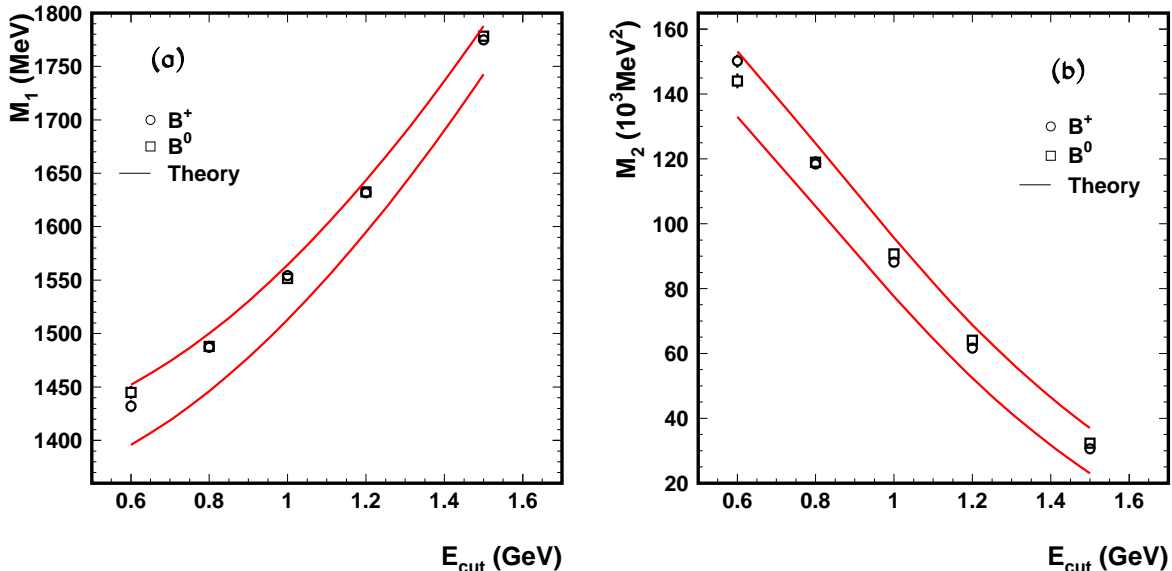


FIG. 7: The first and second electron energy moments, M_1 (a) and M_2 (b), as a function of cutoff energy E_{cut} with the bounds on the theory predictions shown as curved lines. The errors shown are statistical and systematic.

the moments of the hadronic mass distribution, will be used for the determination of the HQE parameters and of $|V_{cb}|$.

Acknowledgments

We thank the KEKB group for the excellent operation of the accelerator, the KEK Cryogenics group for the efficient operation of the solenoid, and the KEK computer group and the National Institute of Informatics for valuable computing and Super-SINET network support. We acknowledge support from the Ministry of Education, Culture, Sports, Science, and Technology of Japan and the Japan Society for the Promotion of Science; the Australian Research Council and the Australian Department of Education, Science and Training; the

National Science Foundation of China under contract No. 10175071; the Department of Science and Technology of India; the BK21 program of the Ministry of Education of Korea and the CHEP SRC program of the Korea Science and Engineering Foundation; the Polish State Committee for Scientific Research under contract No. 2P03B 01324; the Ministry of Science and Technology of the Russian Federation; the Ministry of Education, Science and Sport of the Republic of Slovenia; the National Science Council and the Ministry of Education of Taiwan; and the U.S. Department of Energy.

* on leave from Nova Gorica Polytechnic, Nova Gorica

- [1] I. Bigi, M. Shifman, and N. Uraltsev, *Ann. Rev. Nuc. Part. Sci.* **47**, 591 (1997)
- [2] A. V. Manohar and M. B. Wise, *Phys. Rev.***D49**, 110 (1994).
- [3] P. Gambino and N. Uraltsev, *Eur. Phys. J.* **C 34**, 181 (2004). See also C. Bauer, Z. Ligeti, M. Luke and A. Manohar *Phys. Rev.* **D 67**, 054012 (2003) [hep-ph/0210027]
- [4] M. Battaglia *et al.* (DELPHI Collaboration), DELPHI 2003-028 CONF 648.
- [5] A. H. Mahmood *et al.* (CLEO Collaboration), submitted to *Phys. Rev. D.* [hep-ex/0403053]
- [6] B. Aubert *et al.* (BABAR Collaboration), submitted to *Phys. Rev. D.* [hep-ex/0403030]
- [7] Throughout this paper, the inclusion of the charge conjugate mode decay is implied unless otherwise stated.
- [8] S. Kurokawa and E. Kikutani, *Nucl. Instr. and Meth.* A499, 1 (2003), and other papers included in this volume.
- [9] A. Abashian *et al.* (Belle Collaboration), *Nucl. Instr. and Meth.* A **479**, 117 (2002).
- [10] Events are generated with the CLEO QQ generator (see <http://www.ins.cornell.edu/public/CLEO/soft/qq>); the detector response is simulated with GEANT, R. Brun *et al.*, GEANT 3.21 CERN Report DD/EE/84-1, 1984.
- [11] N. Isgur and D. Scora, *Phys. Rev.* **D 52**, 2783 (1995). See also N. Isgur *et al.*, *Phys. Rev.* **D 39**, 799 (1989).
- [12] J. Duboscq *et al.* (CLEO Collaboration), *Phys. Rev. Lett.* **76**, 3898 (1996).
- [13] J.L. Goity and W. Roberts, *Phys. Rev.* **D 51**, 3459 (1995).
- [14] S. Eidelman *et al.*, *Phys. Lett. B* 592, 1 (2004).
- [15] E. Barberio and Z. Was, *Comp. Phys. Commun.* **79**, 291 (1994).
- [16] F. De Fazio and N. Neubert, *JHEP* **9906** (1999) 017.
- [17] A. Limosani and T. Nozaki, [hep-ex/0407052]
- [18] A. Höcker and V. Kartvelishvili, *Nucl. Instr. Meth.* **A372**, 469 (1996). [hep-ph/9509307]